Cell, Volume *135*

Supplemental Data

Chromosome Congression by Kinesin-5

Motor-Mediated Disassembly

of Longer Kinetochore Microtubules

Melissa K Gardner, David C. Bouck, Leocadia V. Paliulis, Janet B. Meehl, Eileen T. O'Toole, Julian Haase, Adelheid Soubry, Ajit P. Joglekar, Mark Winey, Edward D. Salmon, Kerry Bloom, and David J. Odde

INDEX

Introduction

Supplemental Results:
Figure S1: Mutant kinetochore distributions in wild-type and histone-H3 depletion
Figure S2: Spindle length and kinetochore organization, wild-type vs. *cin8Δ*
Figure S3: Spindle length and kinetochore organization, wild-type, *cin8Δ,* and *bim1Δ*
Table S1: Single-factor ANOVA analysis: cryo-electron microscopy data
Figure S4: Cin8p overexpression results
Figure S5: GFP-tubulin FRAP time series: wild-type vs. *cin8Δ*
Figure S6: Astral microtubule length distributions
Figure S7: Experimental results for *cin8-nlsΔ* cells
Figure S8: Experimental evidence for ATP-driven motor motility
Figure S9: Modeling results: alternate models
Figure S10: Benomyl results
Figure S11: Kip1-GFP spindle localization
Figure S12: Cin8-GFP and Kip1-GFP FRAP by spindle position
Figure S13: "Self-Organized" modeling results

Simulation Methods:
Table S2: Model parameter values: MT dynamics simulations
Table S3: Motor model description
Table S4: Motor model assumptions
Table S5: Motor model parameter values
Table S6: Motor model variables
Table S7: "Self organized" model parameter values: MT dynamics simulations

Experimental Methods:
Table S8: Yeast Strains

Supplemental References

Introduction

During metaphase in the budding yeast mitotic spindle (Fig. 1A) sister mitotic chromosomes (blue) are still physically attached to one another. Each chromosome is mechanically linked via a single kinetochore (cyan) to the plus end of a single kinetochore microtubule (kMT, black) whose minus end is in turn linked to a spindle pole body (SPB, grey) (Goshima and Yanagida, 2000; He et al., 2000; Joglekar et al., 2006; O'Toole et al., 1999; Pearson et al., 2001; Pearson et al., 2004; Winey et al., 1995). The sister chromosome is similarly linked to the opposite SPB. Kinetochores move as their associated kMT plus ends dynamically exchange αβ-tubulin subunits with the soluble pool in the nucleus, while kMT minus end assembly remains non-dynamic (Maddox et al., 2000; Pearson et al., 2006; Tanaka et al., 2005). In all, there are 16 sister chromosome pairs in haploid cells, for a total of 32 kinetochores and 32 kMTs, although for schematic simplicity we show only a single pair in Fig. 1A.

The mechanical linkage that runs from pole to pole via the kMTs and kinetochores is almost always under tension in metaphase (Goshima and Yanagida, 2000; Goshima and Yanagida, 2001; He et al., 2000; Pearson et al., 2001). As a result, kinetochores constrain chromosomes to congress at the equator, provided each kinetochore remains in its respective half of the spindle. Since each kinetochore is persistently attached to a single kMT plus end during metaphase in budding yeast (Gardner et al., 2005; Pearson et al., 2004), kMT plus end assembly must be limited so that each kMT plus end generally remains in its own half-spindle. If subunit exchange at the kMT plus end were unfavorable everywhere in the spindle, then kinetochores would tend to cluster around their respective poles, as the pole would be the most probable position for a kMT plus end. In fact, kinetochores do not cluster near their poles, but instead cluster about midway between their pole and the equator (Gardner et al., 2005; He et al., 2000; Pearson et al., 2006; Pearson et al., 2001; Shimogawa et al., 2006; Sprague et al., 2003; Tytell and Sorger, 2006). Therefore, kMT plus ends should have net assembly favored near the SPBs, but net disassembly near the equator, which together establish a gradient in net kMT assembly.

Through a series of fluorescence and electron microscopy studies, we confirmed the existence of the gradient in net kMT plus end assembly (Gardner et al., 2005; Pearson et al., 2006; Pearson et al., 2004; Shimogawa et al., 2006; Sprague et al., 2003). This gradient is depicted in Fig. 1A as a region near the SPB where net assembly is favorable (green, i.e. when kMTs are relatively short), and another region near the equator where assembly is unfavorable (red, i.e. when kMTs are relatively long). As a result of this gradient in net assembly, kMT plus ends grow efficiently away from poles, but rarely cross the equator. In between these two regions is an intermediate region where net assembly is close to zero, and this region constitutes an attractor zone for kMT plus ends and their associated kinetochores (Fig. 1A, yellow arrows). A key question, that we now address, is how the kMT plus end net assembly gradient is established.

Supplemental Results

Kinetochore Position Distribution: Wild-type, cin8Δ, and kip1Δ

There are two kinesin-5 motors in budding yeast, Cin8p and Kip1p. Kip1p is considered the less important of these two motors (Hildebrandt and Hoyt, 2000; Roof et al., 1992; Saunders et al., 1997; Tytell and Sorger, 2006), as *kip1Δ* phenotypes are less severe than those of *cin8Δ* cells. Nevertheless, we quantified kinetochore organization in *kip1Δ* mutants via Cse4-GFP fluorescence analysis, similar to the analysis for *cin8Δ* mutants. Here, *kip1Δ* mutants had a similar, but moderated, effect on kinetochore organization as compared to *cin8Δ* mutants (Fig. S1A). The peak in kinetochore-associated fluorescence is shifted towards the spindle equator, indicating that kMTs are longer in *kip1Δ* mutants as compared to wild-type spindles. This shift is less significant than in *cin8Δ* mutants, though, suggesting that Kip1p ultimately has a more moderate effect on kMT assembly than Cin8p (Fig. S1A).

Kinetochore Position Distribution Histone H3-repressed Cells: Wild-type, cin8Δ and kip1Δ

To further ensure that reduced spindle length was not responsible for the observed kinetochore organization changes in *cin8Δ* mutants, we repeated the kinetochore localization experiments in histone H3 repression mutants. As reported previously, histone H3 repression results in longer metaphase spindles, apparently by making the chromatin between sister kinetochores more compliant (Bouck and Bloom, 2007). Thus, *cin8Δ* spindles in a histone H3 repressed mutant have lengths typical of wild-type cells (Bouck and Bloom, 2007). In these cells, although the entire range of spindle lengths is within the typical wild-type range, loss of kinetochore clustering and shifting of kinetochores toward the equator are still apparent, similar to *cin8Δ* spindles in a wild-type background (Fig. S1B). Thus, deletion of Cin8p affects metaphase kinetochore organization independent of its role in regulating spindle length.

Although spindle lengths are increased in the histone H3 repressed spindles, *kip1Δ* mutants again show a moderate shift in kinetochore-associated fluorescence towards the spindle equator (Fig. S1B).

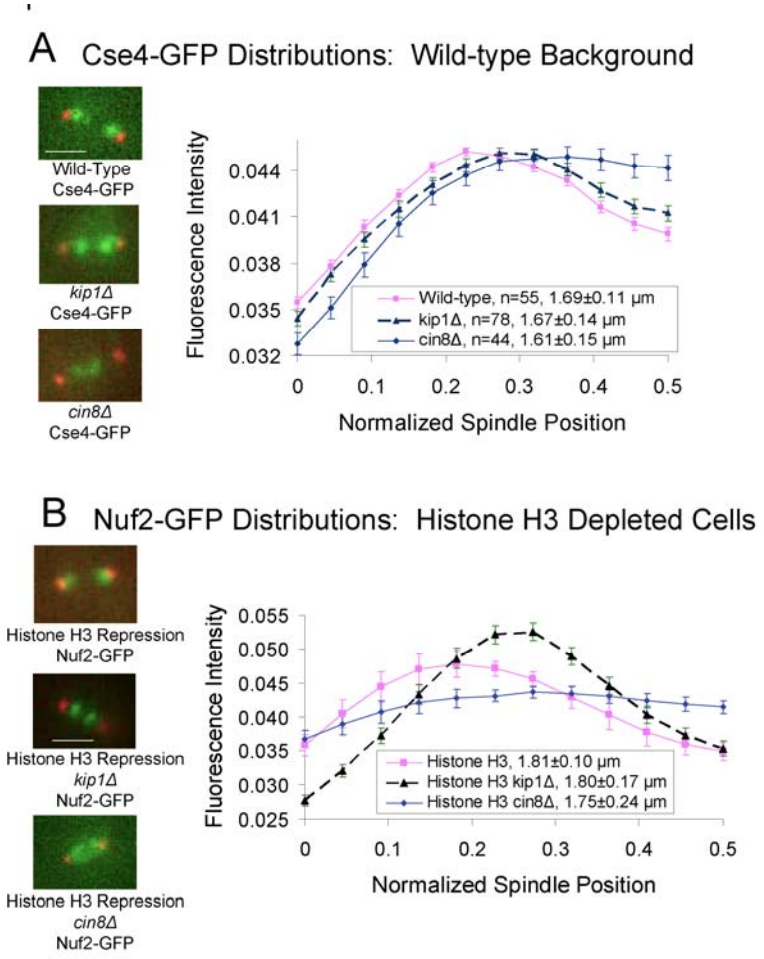

Figure S1: *kip1Δ* mutants have a similar, but attenuated, kinetochore disorganization phenotype as compared to *cin8Δ* mutants. (A) As shown in experimental images (left), kinetochore organization is mildly disrupted in *kip1Δ* mutant spindles (Cse4-GFP, green; Spc29-RFP pole markers, red). By quantifying Cse4-GFP fluorescence over a large number of spindles (right) mean kinetochore positions suggest that kMTs in *kip1Δ* mutants are longer than in wild-type spindles, but shorter than in *cin8Δ* mutant spindles. (scale bar, 500 nm; error bars s.e.m.) (B) Similar results are obtained using histone-repression mutants, where the spindle length is longer than in wild-type spindles.

Spindle length and kinetochore organization, wild-type, cin8Δ, and bim1Δ

In this study, we focused on the regulation of kMT plus-end microtubule dynamics by kinesin-5 molecular motors, independent of their role in generating outward extensional sliding forces on the poles to establish a steady-state metaphase spindle length. As Cin8p and Kip1p are redundant for the microtubule sliding function in yeast, deletion of either molecular motor by itself results in metaphase spindles with either a modest reduction in spindle length (*cin8Δ*) or little change in spindle length (*kip1Δ*) (Fig. S2A). To ensure that our analysis of kMT plus-end dynamics was not affected by differences in spindle lengths between wild-type and mutant cells, we selected a subset of the total distribution of wild-type and *cin8Δ* spindle lengths for analysis (Fig. S2B). This selection was made by selecting all wild-type and mutant spindles within the range of 1.5-1.7 μm for analysis, such that the mean and standard deviation of both wild-type and mutant spindle lengths were similar. This sub-selection represents a substantial fraction of all the spindles (~30-40%), and results in a mean spindle length only slightly different than the mean of the parent population (~5-15% different). A similar process was used for both Cse4-GFP and GFP-Tub1 fluorescence analysis experiments.

For comparison, the Cse4-GFP kinetochore localization analysis was also performed on the entire wild-type and *cin8Δ* spindle length populations (Fig. S2C, left). Although results in the main text are sub-selected to eliminate any spindle length bias in the analysis, nearly identical results were achieved using the entire spindle length population (Fig. S2C, left). In addition, the longest 50% of spindle lengths for both populations were analyzed, with similarly indistinguishable results (Fig. S2C, right).

As an added control, spindle microtubule organization was evaluated in a strain with reduced spindle lengths. In *bim1Δ* mutants, spindle lengths are shorter than in wild-type spindles, with a spindle length distribution that is similar to *cin8Δ* mutant cells (Fig. S3A). However, in contrast to *cin8Δ* mutants, spindle microtubule organization is not disrupted in *bim1Δ* mutants, but rather is similar to the wild-type distribution (Fig. S3B). Thus, we conclude that the disrupted spindle organization in *cin8Δ* mutant cells is not simply a consequence of reduced *cin8Δ* spindle lengths.

A Spindle Length Distribution

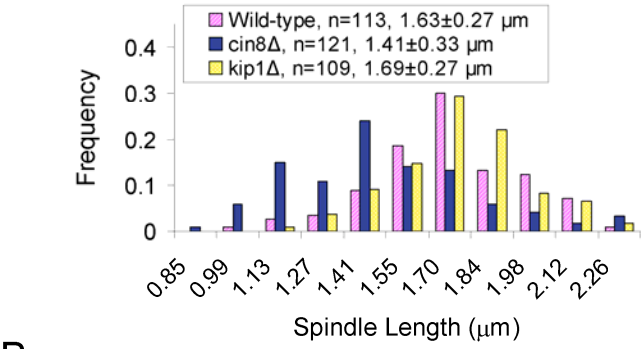

B Spindles Selected for Analysis of Cse4-GFP Distribution

Spindle Type	Spindle Length (µm)	N, All spindles	Spindle Length Selected for Cse4-GFP Analysis (µm)	N, Spindles Selected for Analysis
Wild-type	1.63 ± 0.27[a]	113	1.69 ± 0.11[a]	55
cin8Δ	1.41 ± 0.33[a]	121	1.61 ± 0.15[a]	44

[a]mean ± standard deviation

C Alternate Populations: Cse4-GFP Distribution

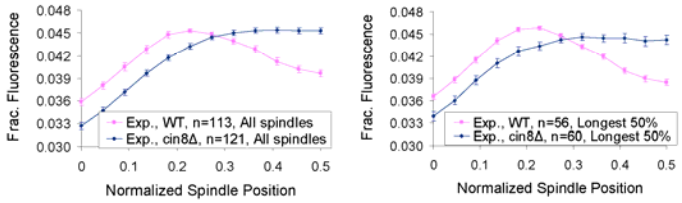

Figure S2: Mutant spindle lengths are moderately shorter than wild-type spindle lengths, although kinetochore organization results are similar regardless of spindle length (A) Spindle length distributions for wild-type, *cinΔ*, and *kip1Δ* spindles. *cin8Δ* spindle lengths are moderately shorter than wild-type spindle lengths. (B) To control for spindle length, a subset of the total distribution of spindles is selected for analysis of kMT dynamics, as shown. (C) Cse4-GFP kinetochore organization analysis of alternate spindle length populations produced similar results.

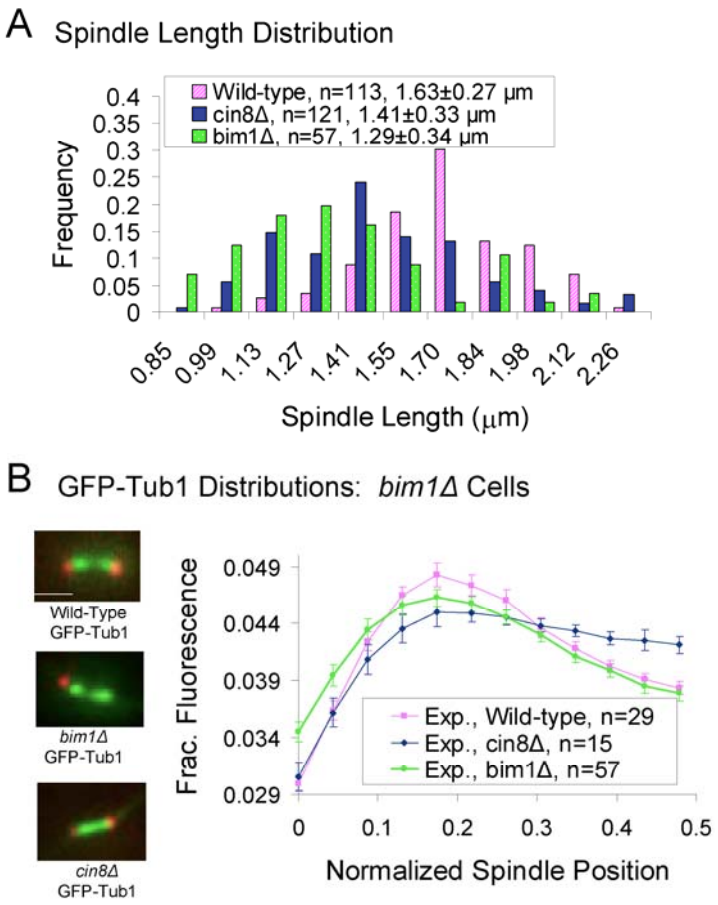

Figure S3: A *bim1Δ* mutant with similar spindle lengths to *cin8Δ* mutants does not have disrupted spindle microtubule organization (A) *bim1Δ* spindle lengths are shorter than in wild-type cells, but similar to *cin8Δ* spindle lengths. (B) GFP-Tub1 organization is similar in wild-type and *bim1Δ* spindles, but disrupted in *cin8Δ* spindles.

ANOVA Analysis of MT Length Distributions Measured via Cryo-Electron Microscopy

A single-factor ANOVA analysis of MT length distributions between cells was performed for the wild-type and *cin8Δ* spindles to ensure that all MT lengths could be analyzed as independent entities (Table S1, below). All cells were statistically indistinguishable from each other.

Table S1: Single-Factor ANOVA Analysis: Wild-type and *cin8Δ* Mutant Spindles

SUMMARY: cin8Δ

Groups	*Count*	*Sum*	*Average*	*Variance*
Cell 01	65	28474	438	111571
Cell 02	60	25952	432	214142
Cell 03	60	22995	383	151855
Cell 04	49	19667	401	137830
Cell 05	50	20388	408	90007

ANOVA: cin8Δ

Source of Variation	*SS*	*df*	*MS*	*F*	*P-value*	*F crit*
Between Groups	124701	4	31175.27	0.219	0.929	2.404
Within Groups	39760636	279	142511.2			
Total	39885337	283				

SUMMARY: Wild-type

Groups	*Count*	*Sum*	*Average*	*Variance*
Cell 01	43	12061	280.4884	67832.87
Cell 02	37	11260	304.3243	120916.2
Cell 03	38	15334	403.5263	395248.5
Cell 04	42	9823	233.881	54929.23

ANOVA: Wild-type

Source of Variation	*SS*	*df*	*MS*	*F*	*P-value*	*F crit*
Between Groups	606519.2	3	202173.1	1.309854	0.273	2.663
Within Groups	24078257	156	154347.8			
Total	24684776	159				

Cin8p Overexpression: Spindle Statistics

Similar to kinesin-5 deletion experiments, overexpression of kinesin-5 sliding motors has an effect on spindle length (Saunders et al., 1997). Here, an increased concentration of sliding motors in the nucleus results in longer spindle lengths (Fig. S4A). Because the Cin8p overexpression assay had a substantial effect on spindle length (Fig. S4A), it was not possible to compare equal spindle lengths between wild-type and Cin8p-overexpression in considering kinetochore organization. Thus, quantitative analysis was performed such that kinetochore fluorescence was recorded as a function of absolute distance from the pole, regardless of spindle length (Fig. S4B). It was found that although spindle lengths were increased, the peak in kinetochore-associated fluorescence was ~50% closer to the poles in spindles with Cin8p overexpression than in control spindles. This result suggests that kMT length is substantially reduced in the presence of high concentrations of Cin8p. The kMT shortening occurs despite the increase in chromatin stretching between sister kinetochores, which by itself promotes kMT assembly (Franck et al., 2007; Gardner et al., 2005; King and Nicklas, 2000). Thus, the effect of Cin8p overexpression and its associated promotion of kMT disassembly is dominant over the tension-dependent promotion of assembly, and so net kMT shortening occurs.

Although the overexpression experiment results in increased Cin8p expression as evidenced by longer spindle lengths and shorter kMTs, it is difficult to predict the expression level quantitatively, and large fluctuations in expression level are likely (Bloom et al., 1998). For this reason, simulation results, although qualitatively predicted in Fig. 1A, are not quantitatively fit to the Cin8p overexpression experiment.

A Cin8p Overexpression: Spindle Statistics

	Wild-Type Control	Cin8p-Overexpression
Number of Spindles Analyzed	N=125	N=96
Spindle Length	1.80 +/- 0.30[a] μm	2.48 +/- 0.96[a] μm
Estimated kMT Length (Mode)	573 nm	248 nm
% Spindle Length Change	---	+38%
% kMT Length Change	---	-57%

[a]mean ± s.d.

B Cse4-GFP Fluorescence in Cin8p Overexpression

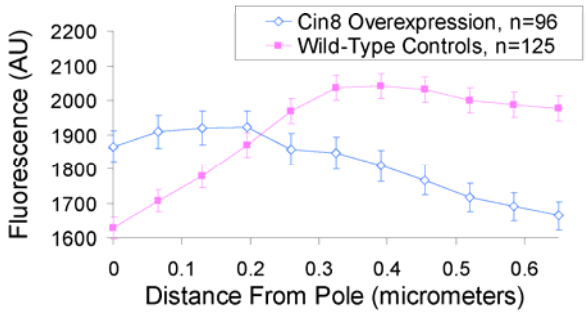

Figure S4: Results for Cin8p overexpression studies. (A) Spindles are longer in Cin8p overexpression cells than in wild-type cells, although the estimated kMT length is reduced. (B) The Cse4-GFP fluorescence distribution as a function of absolute distance from one spindle pole body is similar to normalized results (Fig 1D).

GFP-Tubulin Fluorescence Recovery After Photobleaching: Half-Spindle Time Series Recovery

GFP-Tubulin FRAP is robust in both wild-type and *cin8Δ* cells, as shown by the representative time series in Fig. S5. Recovery obeys a single exponential, and summary statistics are as shown.

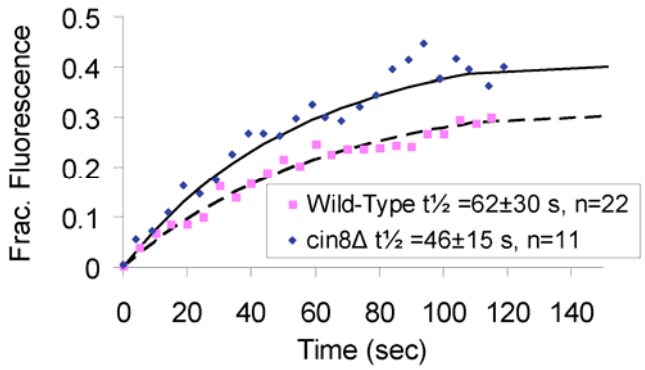

Figure S5: GFP-Tubulin FRAP in wild-type and *cin8Δ* spindles. As shown by the FRAP time series, half-spindle FRAP recovery rate is similar in both wild-type and *cin8Δ* cells (p=0.03), indicating that kMT self-assembly remains dynamic in *cin8Δ* spindles. The extents of recovery are also similar.

Astral Microtubule Length Distributions

In Fig.S6 is shown the distribution of astral microtubule lengths for varying cytoplasmic concentrations of Cin8p. Although the distributions are broad, as expected, the distribution shifts toward increasing aMT length with decreasing Cin8p expression.

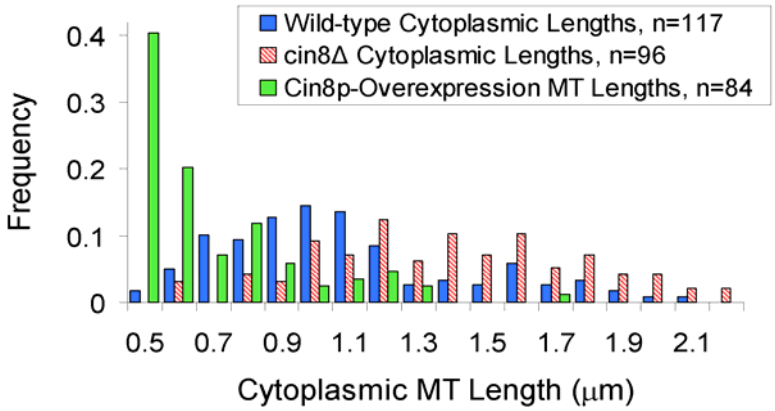

Figure S6: Astral MT length distributions. Astral microtubule lengths are broadly distributed, although there is a shift in mean length depending on the Cin8p expression level. The mean aMT length correlates inversely with Cin8p expression level.

Experimental results for cin8-nlsΔ cells

We performed experiments using a mutant yeast strain in which the Cin8p nuclear localization signal (NLS) is deleted (Hildebrandt and Hoyt, 2001). This mutation reduces the concentration of Cin8p in the nucleus, while increasing the cytoplasmic concentration of Cin8p. Fluorescent mCherry-tubulin images of metaphase spindles with associated aMTs were collected. Analysis of mcherry-tubulin distribution in the spindle produced results similar to *cin8Δ* cells (Fig. S7A). Wild-type spindles had characteristic tubulin "tufts", with a peak in mcherry-tubulin fluorescence roughly midway between each pole and the spindle equator. In contrast, mcherry-tubulin fluorescence in *cin8-nlsΔ* spindles was shifted towards the spindle equator, suggesting that kMT lengths were increased (Fig. S7A). Spindle lengths were reduced in the mutation, similar to *cin8Δ* spindles, although comparable spindle lengths were used between wild-type and mutant cells for the mcherry-Tub1 spindle fluorescence analysis (Fig. S7B). Importantly, and in contrast to *cin8Δ* spindles, aMT lengths in *cin8-nlsΔ* cells were shorter than in wild-type cells (Fig. S7C). In general, the lengths of the MTs in a given compartment, either the nucleus or the cytoplasm, depended inversely on the relative amount of Cin8p in that compartment. This analysis indicates that the effect of Cin8p is mediated locally in a given cellular compartment, rather than globally.

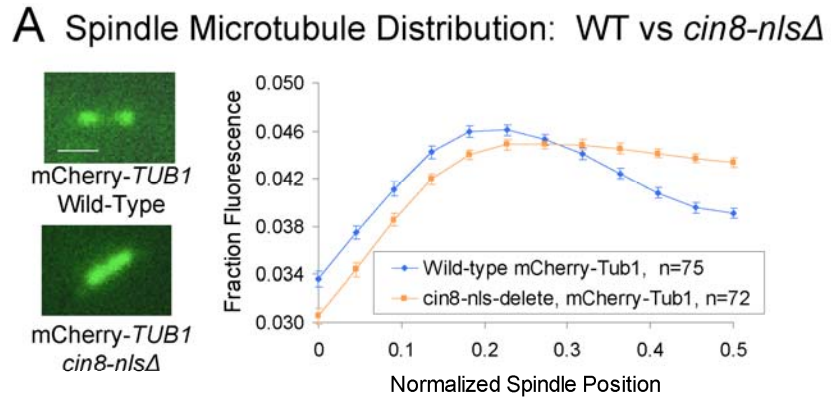

B Spindle Lengths: WT vs *cin8-nlsΔ*

Spindle Type	Spindle Length (μm)	N, All spindles	Spindle Length selected for Analysis in (A) (μm)	N, Spindles Selected for Analysis in (A)
Wild-type	1.46 ± 0.25[a]	75	1.46 ± 0.25[a]	75
cin8-nlsΔ	1.38 ± 0.15[a]	71	1.47 ± 0.08[a]	48

[a]mean ± standard deviation

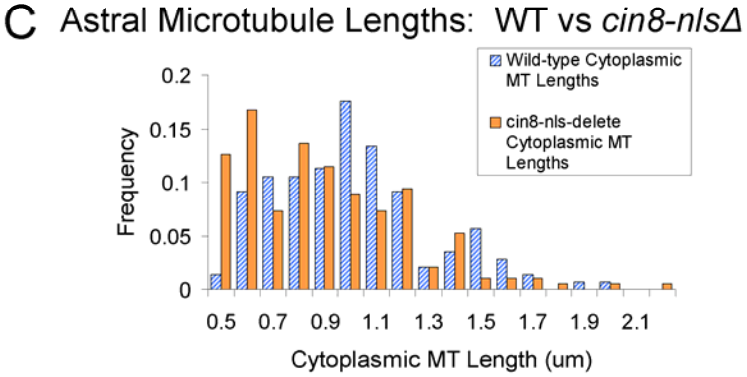

Figure S7: Spindle lengths, kMT lengths, and aMT lengths in *cin8-nlsΔ* spindles. (A) A comparison of mcherry-tubulin fluorescence distributions in wild-type and *cin8-nlsΔ* spindles. As shown in the images on the left, wild-type spindles have characteristic mcherry-Tub1 "tufts" (green) on either side of the spindle equator, while *cin8-nlsΔ* spindles have a single bar of mcherry-Tub1 fluorescence, similar to *cin8Δ* spindles. This result indicates that kMTs are longer in the *cin8-nlsΔ* cells. Quantification over many images produces similar results (right). (scale bar 500 nm, error bars s.e.m.) (B) Similar to *cin8Δ* mutants, spindle length is reduced in *cin8-nlsΔ* mutants, presumably due to the lower concentrations of anti-parallel-attached Cin8p motors that act to exert an outwardly directed sliding force to separate the SPBs. (C) In contrast to *cin8Δ* mutants, overexpression of Cin8p in the cytoplasm of *cin8-nlsΔ* mutants results in shorter aMTs, rather than the longer aMTs observed in *cin8Δ* mutants.

Experimental Evidence for ATP-Driven Motor Activity

Numerous studies have demonstrated that kinesin-5 motors, including Cin8p, have plus-end directed motor activity both *in vitro* and *in vivo* (Gheber et al., 1999; Gordon and Roof, 1999; Hildebrandt and Hoyt, 2000; Kapitein et al., 2005; Kashina et al., 1996; Tao et al., 2006; Valentine et al., 2006). In addition, because of its bipolarity, the kinesin-5 motor Eg5 is capable of cross-linking adjacent MTs and motoring toward the plus ends of each MT, independent of the relative orientation angle between the two MTs (Kapitein et al., 2005). Because of the results of (Kapitein et al., 2005) and the widely recognized torsional compliance of kinesins (Hancock and Howard, 1998; Hunt and Howard, 1993; Kuo et al., 1991), it seems likely that kinesin-5 motors, which are largely regarded as sliding motors that push antiparallel MTs apart, could just as easily cross-link parallel MTs and motor toward the MT plus ends without generating sliding force between the parallel MTs.

To test the simulation assumption that motors walk toward MT plus-ends on parallel microtubules, we performed experiments to provide evidence for ATP-driven motility of kinesin-5 motors in the yeast spindle. As shown in Fig. S8A (left), both simulated and experimental kymographs of spindle Cin8-GFP were generated to examine spindle-associated motor motility over time. Due to the density of motors in the spindle, it was not possible to detect individual Cin8p motility without repeatedly photobleaching to reduce fluorescent motor numbers. However, motor dynamics on the spindle can be inferred from changes in half-spindle Cin8-GFP fluorescence intensity over time. As motors move along the spindle, they would eventually reach the ends of parallel kMTs and soon dissociate. The expected result is that the number of Cin8-GFP molecules will fluctuate over time due to motor-based turnover and movement on the spindle.

If the motor activity were inhibited, then the turnover would be less dynamic, and thus the fluctuations in number would be smaller. To assess whether the Cin8-GFP dynamics on the spindle were affected by inhibition of motor activity, Cin8-GFP spindle kymographs were then obtained for cells treated with azide (Pearson et al., 2003), which will stall motor motility. Quantitative analysis showing the half-spindle standard deviation in Cin8-GFP fluorescence over time for both experiments is shown in Fig. S8B. The variation in Cin8-GFP fluorescence intensity is reduced in azide-containing media as compared to control media, suggesting that motor motility is reduced. Experiments in low-dose benomyl had variability in half-spindle Cin8-GFP fluorescence that was intermediate between control spindles and azide media spindles, suggesting that kMT plus-end dynamics also contribute to motor exchange on the spindle. We conclude that ATP is required for normal Cin8p dynamics, and that the fluctuations in Cin8p on the spindle are consistent with a model that assumes plus-end directed motility along parallel spindle MTs.

As the density of Cin8-GFP motors in the spindle precluded identification of individual motor spindle movements, we then performed experiments in which we repeatedly photobleached spindles labeled with Cin8-3XGFP and then collected rapid time-lapse images of the spindle after Cin8-3XGFP fluorescence redistribution. This method reduced the fluorescent motor number, allowing for detection of individual Cin8-3XGFP movements. As is experimentally observed and is predicted via simulation (Fig.

S8C), motor movements in the spindle are apparent in both directions, as predicted by a model in which with motors walk along parallel kMTs and ipMTs. We observed a bimodal distribution of motor velocities that is consistent with faster intrinsic motor velocities (Fig. S8 C, left, and D), and slower MT polymerization-limited motor velocities (Fig. S8 D, right, and D). The slower velocity values were similar to those observed on astral MTs where aMT assembly rate presumably limits motor velocity at the growing plus end (Fig. S8, D).

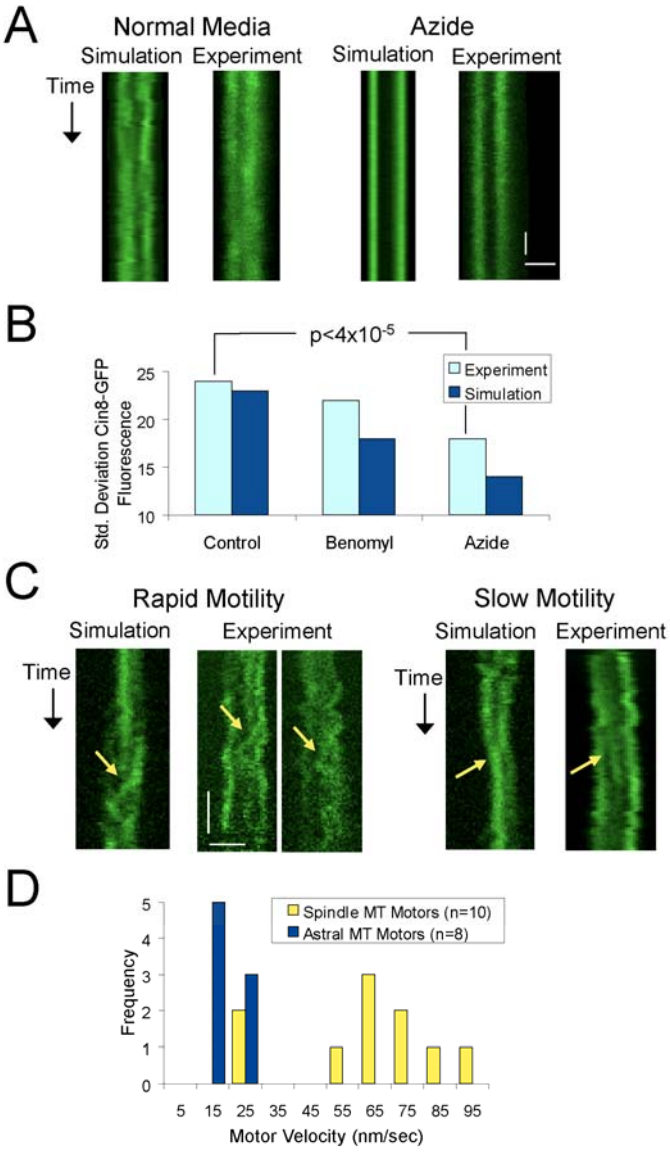

Figure S8: Experimental evidence for ATP-driven motor motility in the spindle. (A) Simulated and experimental kymographs of Cin8-GFP (green) in metaphase spindles over time show clear qualitative differences between Cin8p activity in control media (left) vs azide (right; horizontal scale bar, 1 µm, vertical scale bar, 4 sec) (B) Cin8-GFP kymographs are quantitatively compared by calculating the standard deviation in half-spindle fluorescence over time. The p-value (calculated via F-test) reflects a significant difference in the variation of Cin8-GFP fluorescence intensity over time in control conditions vs. azide. (C) Repetitive photobleaching of Cin8-3XGFP labeled spindles reveals Cin8p motor motility in the spindle. Rapid excursions (left, horizontal scale bar, 1 µm, vertical scale bar, 20 sec) are consistent with intrinsic motor motility on MTs, while slower excursions are consistent with MT-polymerization limited motor motility rates. (right) (D) The measured distribution of motor velocities is approximately bimodal. Slower spindle velocity measurements are consistent with motor motility rates as measured on astral MTs, and faster spindle velocities are consistent with previously measured in vitro motility assays for Cin8p.

Alternate Models

The best fit between experiment and simulation was achieved with a model in which motors randomly attach to microtubules. In this model, motors cross-linking parallel-oriented microtubules walk towards and frequently interact with kMT plus-ends. As shown in Fig. S9, the evidence for motor motility is further supported by simulation results with stationary motors. In this alternate model, motors stochastically attach to and detach from microtubules, without any plus-end directed motion. Quantitative analysis of Cin8-GFP simulation results from the stationary Cin8p motor model (Fig. S9, green line) reveals a predicted Cin8-GFP fluorescence distribution that is inconsistent with the observed Cin8-GFP distribution. Rather, the predicted Cin8-GFP distribution for the stationary motor model is roughly similar to the experimentally observed fluorescence distribution for GFP-Tub1 (main text, Fig. 2A). The similarity in the predicted Cin8-GFP and the GFP-Tub1 fluorescence distributions arises because microtubule polymer density is a major factor in determining motor attachment positions on the spindle. However, the quantitative difference between the stationary motor model Cin8-GFP positions (Fig. S9, green line) and the experimentally measured Cin8-GFP positions (Fig. S9, indigo line) can be accounted for by assuming that Cin8-GFP has plus-end motor activity once attached. Note that if the motor were diffusing on the lattice, rather than actively motoring, then the motor fluorescence distribution would also appear to be very similar to GFP-tubulin fluorescence distribution (not shown).

An alternate model could be one in which motors are stably associated with the kinetochore, acting as "markers" of yeast kMT plus-ends, much like Cse4-GFP or Nuf2-GFP (or any other kinetochore component). In simulations where motors are stably associated with both polymerizing and depolymerizing kMT plus-ends, Cin8-GFP fluorescence is shifted, such that it is essentially coincident with kinetochore-associated fluorescence (Fig. S9, blue line). Thus, the experimentally observed off-set between the peak in kinetochore-associated fluorescence and the peak in motor-associated fluorescence (main text, Fig. 4C) is inconsistent with Cin8p being a stable kinetochore component. Rather, the off-set suggests that dynamic kMT plus-ends increase motor dissociation near to the kMT tip so that the peak of Cin8-GFP fluorescence is shifted toward the pole relative to kinetochore fluorescence.

Another way in which the motor could associate with MTs is via copolymerization with tubulin, and then dissociation subsequent to incorporation into the microtubule lattice. This so-called "tip-tracking" mechanism is hypothesized to be used by EB-1 and other plus-end tip-interacting proteins (+TIPs). However, in this model the Cin8-GFP is again coincident with the kinetochore (results not shown), much like the distribution predicted by the kinetochore-associated model described above, and inconsistent with experimental observation.

The best fit between simulation and experiment is achieved when motors bind to and cross-link kMTs of the same polarity, move towards the kMT plus-ends, and track growing but not shortening plus-ends (Fig. S9, red line). This model results in a steady increase in the Cin8-GFP concentration along the kMT, but a decrease in Cin8-GFP concentration near to where the dynamic kMT plus ends are located (main text, Fig. 4C,D), thus quantitatively predicting the fluorescence distribution of Cin8-GFP using reasonable parameters for the motor (see values below).

Note that in this model Cin8p is allowed to randomly crosslink MTs, with no inherent preference for either parallel or anti-parallel binding. This assumption is consistent with the experimentally observed distribution of Cin8-GFP on the spindle, because if the motor had a preference for crosslinking anti-parallel oriented MTs, then the majority of the Cin8-GFP fluorescence would be located near the spindle equator. Since this is inconsistent with the observed Cin8-GFP localization, we conclude that there is no preference for antiparallel MTs. Instead, the model predicts that a substantial majority of cross-links will be between parallel MTs. This is because in the regions where the polymeric tubulin concentration is highest (i.e. in the vicinity of the pole), there is also a strong parallel alignment (>90% parallel). Near the equator the polymeric tubulin level is lower and alignment is mixed (50% parallel). Thus, the majority of Cin8p is expected to be bound to MTs somewhere between the pole and the kinetochores, and of these a substantial majority will likely cross-link parallel kMTs emanating from the nearby pole. This explanation is entirely consistent with both the Cin8-GFP distribution and the Cin8-GFP FRAP, including FRAP resolved by position (see below).

Kinesin-5 motor crosslinking of MTs only affects the model via the effect that crosslinking has on the ability of the motor to consistently interact with the MT plus-ends. Thus, in the kMT-dense spindle, even motors simulated with relatively low individual head processivity will tend to rebind to a nearby MT while the second head remains attached, so that the motor is less likely to completely dissociate from the spindle. Therefore, the "effective" motor processivity is increased due to motor crosslinking (Valentine et al., 2006), ensuring that Cin8p motors frequently interact with the plus-ends of kMTs. A non-crosslinking motor would require a higher intrinsic processivity to consistently arrive at the plus-ends of longer MTs. So, although cross-linking will affect the motor interaction with kMT plus ends, it is not an essential component of the model and can be compensated for by changing other parameters within reasonable limits.

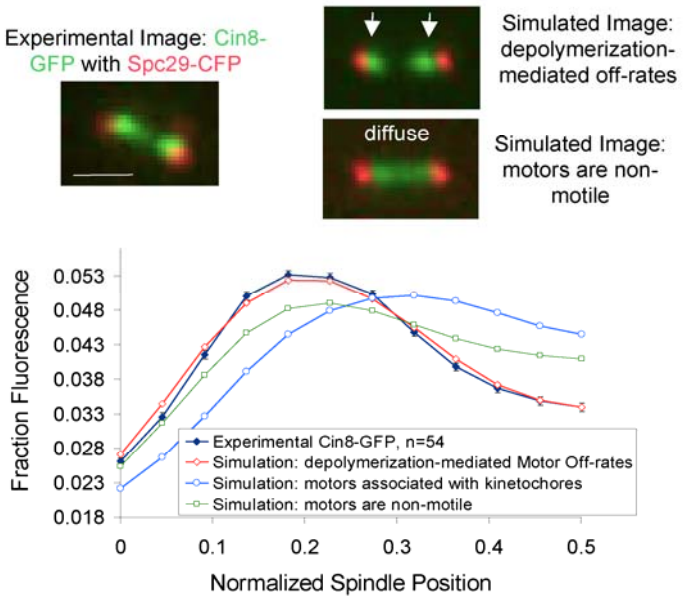

Figure S9: Alternate models for Cin8p dynamics. Alternate models were considered for Cin8p behavior relative to dynamic spindle microtubules. For example, simulated motors that were non-motile (green line), or those that tracked both polymerizing and depolymerizing plus-ends (blue line) had distinct simulation results that differed from the experimentally observed Cin8-GFP fluorescence distribution. The only model considered that was consistent with the experimental Cin8-GFP distribution was one in which motors tracked polymerizing but not depolymerizing kMT plus-ends (red line) (scale bar 1000 nm).

Experimental testing of the motor model: Experimental Benomyl Treatment

In the motor model, motor detachment is largely mediated by disassembling kMTs. If the kMT disassembly rate were reduced, then motors should, on average, be bunched closer toward kMT plus ends and their turnover rate on the spindle should decrease. To test the first prediction, low-dose benomyl was used to experimentally stabilize kMT plus-end dynamics (Pearson et al., 2003), and then the Cin8-GFP distribution was measured relative to kinetochores. As shown in Fig. S10A, Cin8-GFP clusters are nearly coincident with kinetochores in conditions of low-dose benomyl. To quantitatively measure the mean positions of motor and kinetochore clusters, fluorescence centroids were calculated as previously described (Odde and Hawkins, 1997) for Cin8-GFP and Ndc80-Cherry in each half-spindle. The distance between Cin8-GFP and Ndc80-Cherry centroids in control media was 54 ±2 nm (mean ± s.e.m., n=154 half-spindles), while the centroid separation was 19 ±3 nm in benomyl (n=78 half-spindles, $p<10^{-37}$; distribution shown in Fig. S10A).

To test the second prediction, we measured the Cin8-GFP FRAP half-time in control and benomyl-treated cells. As predicted by the motor model and shown in Fig. S10B, the $t_{1/2}$ for Cin8-GFP FRAP is increased where kMT plus-ends are located in benomyl-treated cells as compared to controls. We conclude that the experimentally observed Cin8-GFP distribution and dynamics are sensitive to kMT plus end dynamics, both of which are explained in the motor model by the assumption that motors fail to remain attached to shortening kMT plus ends. Furthermore, the observed motor sensitivity to kMT plus end assembly dynamics indicates that motors interact frequently with kMT plus ends.

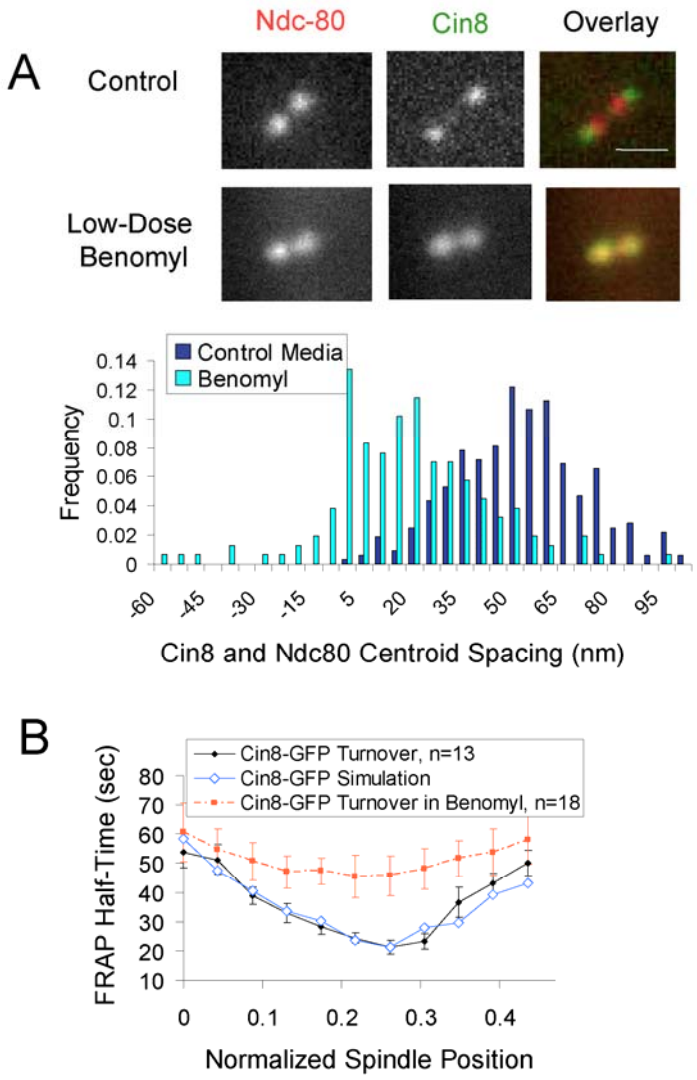

Figure S10: Cin8-GFP localization and dynamics in benomyl-treated cells (A) Cin8-GFP is nearly co-localized with kinetochores in spindles with benomyl-stabilized kMT plus-ends, as shown by the distribution of centroid spacing between Cin8-GFP and Ndc80-Cherry in spindles with dynamic kMT plus-ends (control media, indigo), and stabilized plus-ends (Benomyl, cyan). Modeling suggests that the observed off-set between kinetochore fluorescence and Cin8-GFP in conditions with dynamic kMT plus-ends is due to increased motor off rates from depolymerizing kMT plus-ends. (scale bar 500 nm) (B) Benomyl-stabilized kMT plus-ends results in Cin8-GFP FRAP half-times that are increased in the location of plus-end clustering relative to control cells. (error bars, s.e.m.)

Kip1-GFP Spindle Localization

As shown in Fig. S11, Kip1-GFP localization in the spindle is qualitatively similar to Cin8-GFP. However, Kip1-GFP is more diffuse than Cin8-GFP, suggesting that Kip1p affinity for MTs is lower than for Cin8p.

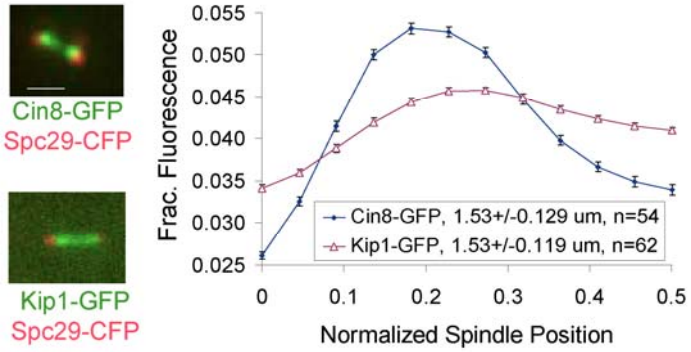

Figure S11: Experimental Kip1-GFP fluorescence distribution in the spindle. The Cin8-GFP spindle fluorescence distribution (indigo line) is more tightly focused than Kip1-GFP distribution (maroon line). This result suggests that Cin8p has a higher affinity for microtubules than Kip1p, such that Cin8p has longer run lengths and thus concentrates more efficiently at the growing kMT plus-ends. Low affinity of Kip1p for MTs may result in short motor run lengths that decrease the likelihood of motor concentration at kMT plus-ends. (scale bar 1000 nm)

Kinesin-5 Motor Turnover on the Spindle

By measuring Cin8-GFP FRAP half-time as a function of spindle position (Fig. S12, green line, we find that Cin8-GFP turns over most rapidly in the position of kMT plus-end clustering, suggesting that dynamic kMT plus-ends mediate motor off-rates. Kip1-GFP turnover (Fig S12, violet line) is also most rapid where kMT plus ends are located. In addition, Kip1-GFP recovery is on average more rapid than Cin8-GFP turnover, again suggesting that Kip1p has a lower affinity for microtubules than Cin8p.

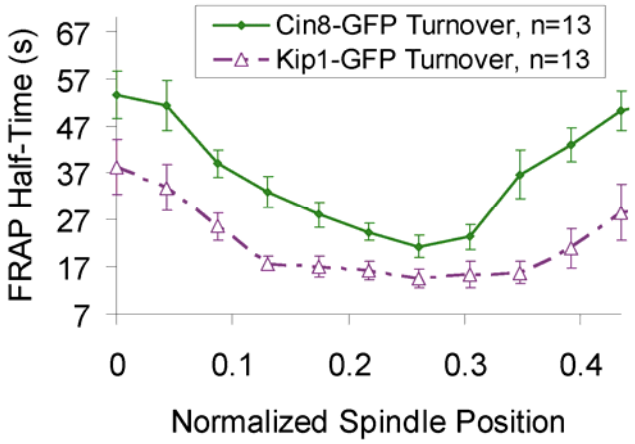

Figure S12: Cin8-GFP and Kip1-GFP FRAP, resolved by spindle position. As was previously reported, FRAP half-time can be resolved by spindle position for GFP-tubulin(Pearson et al., 2006). There is a gradient in GFP-tubulin recovery half-times, such that recovery is most rapid in the location of kMT plus-end clustering (position 0.25). There is a similar gradient in Cin8-GFP FRAP half-times (green line), suggesting that kMT plus-end dynamics mediate Cin8p motor off-rates. Kip1-GFP FRAP half-time obeys a similar gradient as well. However, Kip1-GFP turns over more rapidly than Cin8-GFP, consistent with a model where Kip1p has a lower affinity for MTs, and thus interacts less frequently with kMT plus-ends. (error bars, s.e.m.)

A "Self-Organized" Model: Kinetochore Organization

In previous work, (Gardner et al., 2005; Sprague et al., 2003) kMT dynamics were modeled using an imposed "catastrophe gradient". Although the kMT dynamics simulations in Figures 1-6 were performed as described previously, the results in Fig. 7 and Fig. S13 are the result of a "self-organized" model (see also supplemental movie 5), in which the presence of kinesin-5 motors on kMT plus ends is assumed to increase the catastrophe frequency proportionally to their number at the plus end (see detailed description of model below in the methods section). We have used this self-organized model to test our hypothesis that, by this mechanism, kinetochores could self-organize into the characteristic bi-lobed metaphase configuration of kinetochores.

Typical results from the "self-organized" model are shown in Fig. S13(A). In this model, both experimental wild-type Cin8-GFP localization as well as the experimentally observed bi-lobed Cse4-GFP kinetochore organization are qualitatively reproduced in simulation. In addition, by reducing the number of motors, such as in a *cin8Δ* mutant in which only Kip1p remains, the gradient in motor localization at the kinetochore is disrupted (Fig. S13B), and thus the experimentally observed disruption of kinetochore disorganization is qualitatively reproduced by the model (Fig. S13C). Similarly, by increasing the number of motors in the simulation, such as in the Cin8p-overexpression experiment, the experimentally observed depolymerization of kMTs can be qualitatively reproduced by the model (not shown). Therefore, it is no longer necessary to externally impose a catastrophe gradient on the system, but rather the catastrophe gradient is now a natural consequence of a model where kinesin-5 motors walk to plus ends and promote net disassembly upon arrival. Note that the model makes no assumption about whether the motor itself promotes disassembly, or whether it requires a cargo.

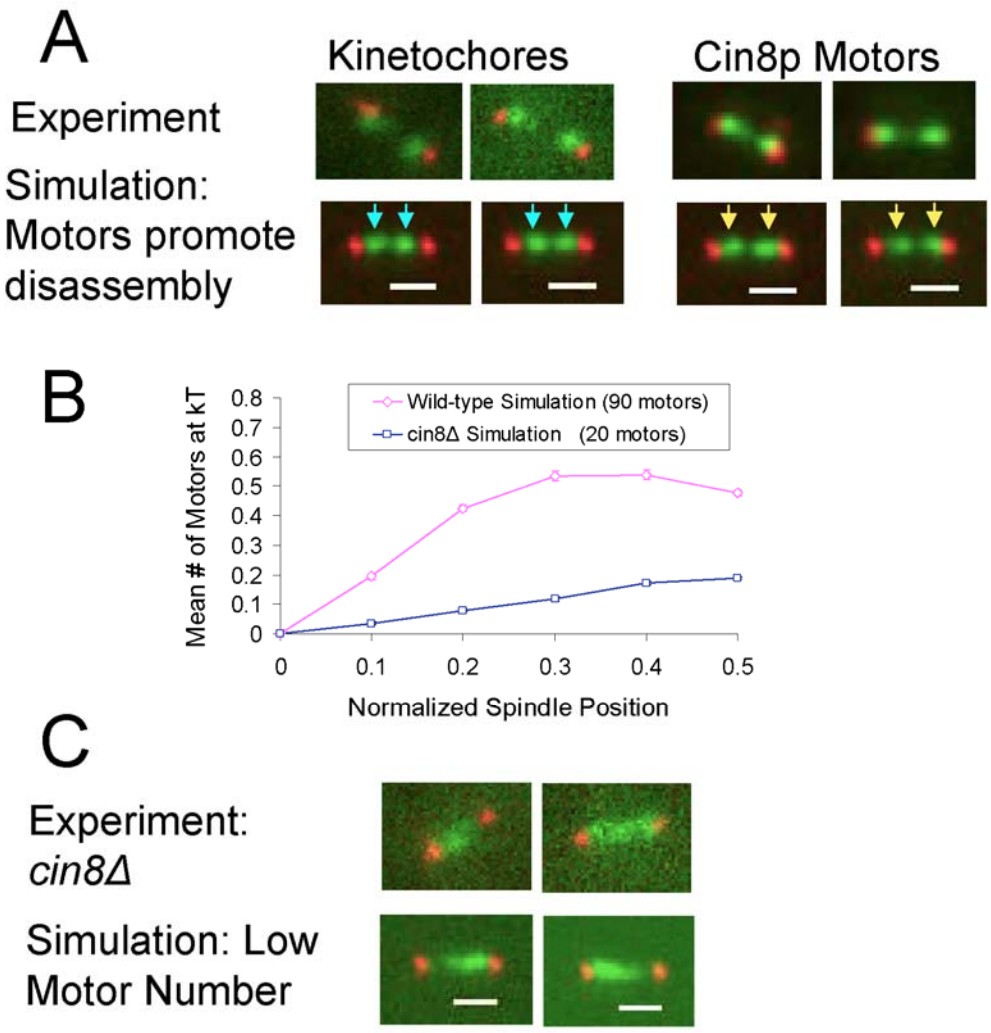

Figure S13: Self-Organized model (A) Experimental Cse4-GFP localization as well as the experimental Cin8-GFP distribution is qualitatively reproduced via a "self-organized" model in which Cin8p promotes net disassembly at the kMT plus end. (scale bar, 1000 nm) (B) By altering the number of simulated motors, the gradient in motor presence at the kinetochore is reduced (indigo line, simulating *cin8Δ* mutants), and (C) kinetochore organization is disrupted, similar to experimental results (scale bar, 1000 nm).

Simulation Methods

A stochastic simulation was developed to account both for dynamic kMT plus-ends in the yeast metaphase spindle as well as for dynamic plus-end directed kinesin-5 motors that interact with MTs, as described below.

Microtubule Dynamics: Model Description

As was previously described (Gardner et al., 2005; Sprague et al., 2003), a Monte Carlo simulation was developed and run in MATLAB to simulate kMT plus-end dynamics. The model assumes that kMT plus-ends remain in one of two states, growing or shortening, at all times. Thus, their dynamics can be fully described via the four parameters of dynamic instability, where V_g and V_s describe rates of kMT plus-end polymerization and depolymerization, respectively, and k_c and k_r describe the probability of switching between these two states. Here, k_c is defined as catastrophe frequency, which is the rate at which a kMT plus-end will switch from a growing state to a shortening state, and k_r is defined as rescue frequency, which is the rate at which a kMT plus-end will switch from a shortening state to a growing state. Previously, we found that there does not exist a constant set of dynamic instability parameters that is able to reproduce kMT plus-end localization in the yeast metaphase spindle (Sprague et al., 2003). Rather, catastrophe and/or rescue frequency vary spatially along the length of the spindle in the model, with net assembly promoted for kMT plus-ends near the pole, i.e. when kMTs are relatively short, and net disassembly promoted for kMT plus-ends near the equator, where kMTs are relatively long (Gardner et al., 2005; Sprague et al., 2003).

All wild-type simulations of kMT plus-end dynamics were run with models and parameter values as previously described (Gardner et al., 2005), and as shown in Table S2. Here, rescue frequency is regulated by tension between sister kinetochores, as measured by the separation distance along the spindle axis between the tips of sister kMTs. Thus, this tensile force, $F_{tensile}$, is defined as:

$$F_{tensile} = \rho^{*}(s - s_0) \qquad (1)\ \text{(Sprague et al., 2003)}$$

Where ρ* is a Hookean spring constant for chromatin connecting sister kMTs with units μm^{-1}, s is the separation distance between the tips of sister kMTs, and s_0 is the rest length of the chromatin. Using this equation, rescue frequency is calculated as a function of tension between sister kinetochores at every time step using the equation:

$$k_r = k_{r,0} \exp(F_{tensile}) \qquad (2)\ \text{(Sprague et al., 2003)}$$

In addition, catastrophe frequency in all simulations (except the final "self-organized" model) was calculated using a theoretical "chemical gradient" model, where k_c varies according to:

$$k_c = k_{c,0} + \beta c_B \qquad (3)\ \text{(Sprague et al., 2003)}$$

Where β is an adjustable parameter that describes the magnitude of the catastrophe promotor's effect, and c_B is the concentration of a theoretical catastrophe promoter. In the model, c_B varies by spindle position via a reaction-diffusion process, in which the

concentration of the theoretical catastrophe promoter is highest at the spindle equator and lower elsewhere (Sprague et al., 2003).

kMT dynamics in *CIN8* deletion experiments were simulated by modifying the catastrophe gradient model to decrease the parameter β, with model parameters as listed in Table S2. The best fit between experiment and theory was achieved with values for MT plus-end growth and shortening rates that were slightly higher than in wild-type simulations (Fig. 2E and Table S2), which decreases FRAP half-times at all spindle positions in simulations of the *cin8Δ* GFP-Tub1 FRAP experiment. These results suggest that Cin8p may also have a slight effect on the suppression of plus-end growth and shortening velocities.

The parameters in Table S2 were used for simulations across all experiments as shown in Figures 1-6.

Non-kMTs (ipMTs) were modeled both using non-dynamic plus-ends, and using a model in which $k_r >> k_c$, with constant values of V_g and V_s. The model for ipMT dynamics did not have a significant effect on simulation results where kMT density is high (not shown, but reviewed in (Pearson et al., 2006)(supplemental material)).

Table S2: Model for kMT Dynamics: Simulation Parameters

Category	Symbol	Description	Wild-Type	*cin8Δ*
Parameter	ρ^*	Chromatin spring constant (μm^{-1})	0.9	0.9
Parameter	$k_{r,0}$	Basal rescue frequency (min^{-1})	9	9
Parameter	$k_{c,0}$	Basal catastrophe frequency (min^{-1})	0.25	0.25
Parameter	β	Catastrophe sensitivity factor for theoretical catastrophe promoter at kinetochore ($M^{-1}min^{-1}$)	680	300
Parameter	Vg	Growth Rate (Vg) ($\mu m/min$)	1.2[a]	1.9[a]
Parameter	Vs	Shortening Rate (Vs) ($\mu m/min$)	1.2[a]	1.9[a]
Parameter	N_{kMT}	Number of kMTs	32	32
Variable	k_c	Catastrophe Frequency (min^{-1})	0.25-30[b]	0.25-15[b]
Variable	k_r	Rescue Frequency (min^{-1})	9-24[c]	9-13[c,d]

[a]In all simulations, growth and shortening rates are assumed to be equal. GFP-Tub1 FRAP experiments constrain growth and shortening values in both wild-type and *cin8Δ* experiments.
[b]Catastrophe frequency depends on spindle position of kinetochore, as described in equation (3) and (Sprague et al., 2003)
[c]Rescue frequency is dependent on distance between sister kinetochores, such that high tension at the kinetochore promotes rescue, as described in equations (1) and (2) and (Gardner et al., 2005).
[d]In the *cin8Δ* simulation, tension-dependent rescue frequency decreases near to basal (no tension) values as a natural consequence of reduced sister kinetochore separation distances.

Kinesin-5 Motor Dynamics: Model Description

A simulation was developed to explicitly model individual kMT dynamics as well as the dynamics of individual MT-associated homotetrameric kinesin-5 molecular motors, based on known properties of the motors (Kapitein et al., 2005; Kashina et al., 1996; Tao et al., 2006; Valentine et al., 2006). Each kinesin-5 homotetramer is modeled as a bipolar motor that has two motor "heads", one at each end of the complex, with each "head" consisting of a pair of motor head domains. As shown schematically in Table S3, one motor head stochastically attaches to an individual MT (at rate k_{on}^*), and subsequently crosslinks via the other head to an adjacent MT (at rate αk_{on}^*). Once bound, motor heads move toward their respective MT plus ends (at velocity v), and eventually detach (each head detaching at rate k_{off}). The motor velocity is slowed by opposing force (Table S3) (Gheber et al., 1999; Valentine et al., 2006), and motor off-rate increases with increasing force (Korneev et al., 2007; Valentine et al., 2006). Additional model assumptions are reviewed in Table S4, with variables and parameter values specified in Tables S5 and S6.

Load-dependent motor velocity results in two distinct motor behaviors depending on whether motors are crosslinking parallel oriented or anti-parallel oriented MTs. As shown in Table S3 (top), motor heads crosslinking anti-parallel oriented MTs walk in opposite directions, stretching the motor and quickly increasing load. Thus, these motors are stationary on the spindle, and tend to concentrate in locations with increased density of anti-parallel MTs, such as at the spindle equator (supplemental movies 3,4). Because

of the increasing load, motors bound to antiparallel MTs tend to detach more rapidly than motors bound to parallel MTs. In contrast, motor heads crosslinking parallel-oriented microtubules walk together towards the plus-ends of both microtubules (Table S3 (top), supplemental movies 3,4). In this case, these motors do not stretch or generate load, but rather walk along the spindle at the unloaded motor velocity. In simulation, it is this behavior that results in the experimentally observed concentration of motors near the plus-ends of kMTs in the yeast mitotic spindle. Once one of the motor heads reaches the plus end, the head is assumed to travel at the rate of MT plus end growth, which is likely to be slower than the unloaded motor velocity(Carminati and Stearns, 1997; Gheber et al., 1999; Gupta et al., 2002; Gupta et al., 2006). The differing rates for each of the two heads results in motor stretching and thus increases the detachment rate. If a plus end undergoes catastrophe, then any motor heads that are at the plus end are assumed to detach. Motor heads that encounter shortening plus ends are also assumed to detach.

Table S3: Model for Kinesin-5 Motor Behavior

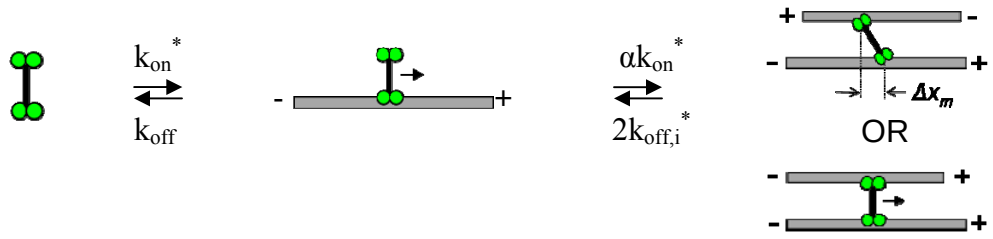

Behavior	Model Equation	Variables	Parameters
Motor Head Attachment	$k_{on}^* = k_{on}$ [Tubulin]	k_{on}^* = motor on-rate constant	[Tubulin] = polymer concentration α = second head on-rate correction
Motor Head Movement	$v_i = v_u(1 - F_{L,i}/F_{stall})$	v_i = motor velocity $F_{L,i}$ = motor tension	F_{stall} = stall force v_u = unloaded velocity
Motor Stretching	$F_{L,i} = \rho_{motor} \Delta x_m$	Δx_m = stretch distance	ρ_{motor} = spring constant
Motor Head Detachment	$k_{off,i}^* = k_{off} e^{(FL,i / Fc)}$	$k_{off,i}^*$ = motor off-rate constant (force dependent)	F_c = critical force k_{off} = unloaded off-rate constant

Kinesin-5 Motor Dynamics: Model Assumptions

Model assumptions for simulation of kinesin-5 motor dynamics are summarized in Table S4, along with references and explanations.

Table S4: Model Assumption Summary

Behavior	Model Assumption	Reference or Explanation
First Head Motor Attachment	Weighted random attachment of first head along spindle according to local MT density	Diffusion in the nucleoplasm is expected to be fast relative to motor rebinding time. In simulation, x_{rms} ~ 2 μm prior to motor rebinding, length of spindle ~1.5 μm.
Second Head Motor Attachment	Random attachment of second head within a 40 nm radius of first head due to torsional flexibility of motor	(Kashina et al., 1996) (Kapitein et al., 2005) (Tao et al., 2006)
Motor Attachment and MT Polarity	No preference of motor attachment to parallel vs anti-parallel attachments, or to kMTs vs the non-kMTs that generally run the length of the spindle (interpolar MTs)	(Kapitein et al., 2005) In general, the metaphase Cin8p motor distribution roughly mirrors MT density rather than enrichment of motors at the midzone
Motor Movement: Force	Motor heads move according to a force-velocity relationship	(Valentine et al., 2006)
Motor Movement: Compliance	Motors act as Hookean springs	(Lee et al., 2006)
Motor Movement: Velocity	Singly-attached motors move at unloaded velocity	By definition
Motor Detachment: Both heads Attached to Adjacent MTs	Motor detachment is force dependent	(Korneev et al., 2007) (Valentine et al., 2006) (Bell, 1978) (for review, see (Evans and Calderwood, 2007))
Motor Detachment: Single Attachments	Singly-attached motors detach at unloaded off-rate	By definition

Kinesin-5 Motor Dynamics: Parameter Value Summary

All simulated parameter values are summarized in Table S5, along with references and explanations. Average numbers of kinesin-5 motors on the mitotic spindle were experimentally determined for this study via analysis of fluorescence intensity (as described in (Joglekar et al., 2006)). We found that ~50 Cin8p motors and ~20 Kip1p motors are bound at any given time to the spindle.

In addition, Cin8p FRAP studies generally constrained motor off-rates in the simulation. Here, the model value for k_{off} was a 'fitting parameter' that was adjusted to reproduce Cin8-GFP spindle localization and FRAP half-times. For Cin8p movement along astral microtubules, the motor appears to processively walk along astral microtubules for 30-60 seconds (500-1000 nm), while the single-head k_{off} modeling parameter would predict single-head run lengths of 3-4 seconds. Because Cin8p is a homotetrameric crosslinking motor, though, motors with a relatively low individual head processivity may tend to rebind to a nearby MT while the second head remains attached, increasing the observed effective processivity of the motor (Valentine et al., 2006). Thus, it may be that motors observed walking along astral microtubules are in fact crosslinking two microtubules. Consistent with this interpretation of the results, recent *in vitro* studies measured a k_{off} of 12 sec^{-1} for Eg5, which is larger than the Cin8p simulated value of 0.3 sec^{-1}, even though the measured k_{off} on astral microtubules is ~0.02 sec^{-1} (Valentine et al., 2006). Therefore, the "effective" motor processivity may be increased due to either motor crosslinking or differing biochemical conditions in the various intracellular compartments/in vitro assays.

A free parameter (α) was defined to account for the diffusion and attachment of a second Kinesin-5 motor head once the first head has attached. The value of this parameter depends on the density of microtubules near the first-head attachment site, and is calculated as follows:

$$\alpha = \frac{\rho_M}{3} \qquad (4)$$

where α is the correction factor, and ρ_M equals the number of neighboring MTs (within a 40 nm radius in the yz plane) that are of sufficient length to allow for crosslinking of the motor at the first head location. In this way, the second head on-rate constant is moderately increased as compared to the first head on-rate constant, depending on the number of MTs in the vicinity of the first head attachment point.

A velocity of 50 nm/sec was used for Cin8p in simulations, to be consistent with *in vitro* measurements of Cin8p motility (Gheber et al., 1999). We hypothesize that the observed motor motility on astral MTs may be limited by MT polymerization, an interpretation that is consistent with the *in vivo* data obtained at rapid temporal resolution on Cin8p motors in the spindle (Fig. S8). The value used in simulation is similar to the measured values for motor motility in the spindle (Fig. S8).

All remaining parameter values are based on previous studies, as described in Table S5.

Kinesin-5 Motor Dynamics: Variable Summary

Typical values for model variables, resulting from the equations in Table S3 and the parameter values described in Table S5, are listed in Table S6. In general, modeling results were highly sensitive to the rules for motor behavior at kMT plus-ends, and it was necessary that parallel-attached motors were motile in order to reproduce experimentally observed motor localization. Simulation of motor FRAP experiments constrained motor off-rates, although on-rates are high enough that many of the simulated motors are attached throughout the simulation. Thus, parameter values and the resulting variable values were not highly constrained to narrow ranges, and it was possible to reproduce both motor localization and FRAP experiments with physically reasonable numbers.

Table S5: Model Parameter Value Summary

Symbol	Description	Typical Value	Reference or Source
v_u	Unloaded Motor Velocity	50 nm/sec	(Gheber et al., 1999) 57 nm/sec
F_{stall}	Motor Stall Force	6 pN	(Valentine et al., 2006), 5-7 pN
ρ_{motor}	Motor Spring Constant	0.5 pN/nm	(Kawaguchi and Ishiwata, 2001)
k_{off}	Unloaded Motor Off-rate Constant	0.3 sec^{-1}	Model Fit Parameter (via FRAP)
k_{on}	Motor On-rate Constant	1 $\mu M^{-1}sec^{-1}$	(Northrup and Erickson, 1992)
N_m	Number of Cin8p Spindle Motors	50	This study (via counting)
α	Second-head on-rate correction	0 – 8	Free parameter, depends on number of MTs in 40 nm attachment radius
r_M	Radius of 2nd Motor Head attach point relative to 1st Motor Head attach point	40 nm	(Kashina et al., 1996) (53 nm)
F_c	Critical Force for force-dependent off-rates	6 pN	(Valentine et al., 2006), 5-7 pN (Korneev et al., 2007), 2 pN

Table S6: Model Variable Summary

Symbol	Description	Typical Value
v_i	Velocity of i^{th} motor	0-50 nm/sec
$N_{m,att}$	Number of attached motors	~50
$F_{L,i}$	Load force on i^{th} motor	0 – 6 pN
$\Delta x_{m,i}$	Stretch of i^{th} motor in the x direction	0 - 30 nm
$k_{off,i}^*$	Force corrected off-rate constant for i^{th} motor	0.3 – 1.0 sec^{-1}
$k_{on,1}^*$	Pseudo first-order motor on-rate constant, 1st head	30-35 sec^{-1}
$k_{on,2}^*$	Pseudo first-order motor on-rate constant, 2nd head	0-500 sec^{-1}
[Tub]	Concentration of tubulin polymer in nucleus [=(1600 units/μm)x(total MT polymer length in μm), assuming a 1.5 μm diameter nucleus]	30-35 μM

Simulation Methods: "Self-Organized" Model

The effect of kinesin-5 motors on catastrophe frequency at kMT plus-ends is modeled according to the following:

$$k_c = k_{c,0} + \beta_m M_T \qquad (5)$$

where k_c is the catastrophe frequency for a given kMT plus-end, $k_{c,0}$ is the basal rescue frequency in the absence of kinesin-5 motors, M_T is the total number of kinesin-5 motors within 16 nm (1st or 2nd tubulin subunit) of the plus-end, and β_m is the sensitivity factor for the effect of motors on basal catastrophe frequency. Model parameter values and typical variable values for the results shown in Fig. S13 and Fig. 7 are shown in Table S7. Cin8p motor parameters and variables are as listed in Tables S3-S6. In addition to the model assumptions outlined in Table S4, kMT plus-end catastrophe frequency is increased upon sister kinetochore crossing, which is unlikely to occur *in vivo* due to steric hindrance of kinetochores and chromatin (Gardner et al., 2008).

Table S7: "Self-Organized" Model for MT Dynamics: Simulation Parameters

Category	Symbol	Description	Wild-Type	*cin8Δ*
Parameter	$k_{c,0}$	Basal Catastrophe Frequency (no Motor) (min^{-1})	0.25	0.25
Parameter	β_m	Catastrophe Sensitivity Factor per Motor at Kinetochore (min^{-1})	20	20
Parameter	Vg	Growth Rate (μm/min)	1.2[a]	1.9[a]
Parameter	Vs	Shortening Rate(μm/min)	1.2[a]	1.9[a]
Parameter	N_{kMT}	Number of kMTs	32	32
Variable	k_c	Catastrophe Frequency (min^{-1})	0.25-30[b]	0.25-10[b]
Variable	M_T	Total Number of Motors at kinetochore	0.5±0.9[c] (out of 90 motors)	0.1±0.4[c] (out of 20 motors)[e]
Variable	k_r	Mean Rescue Frequency (min^{-1})	9-24[d]	9-13[f,d]

[a]In all simulations, growth and shortening rates are assumed to be equal.
[b]Catastrophe frequency depends on the number of motors near the kinetochore, as described in equation (5)
[c]mean±sd per kinetochore (typical in simulation)
[d]Rescue frequency is dependent on distance between sister kinetochores, such that high tension at the kinetochore promotes rescue, as in Gardner et al., 2005.
[e]In the *cin8Δ* simulation, Kip1p motors are still present, and so a smaller number of kinesin-5 motors are simulated.
[f]In the *cin8Δ* simulation, tension-dependent rescue frequency decreases near to basal (no tension) values as a natural consequence of reduced sister kinetochore separation distances).

Table S8: Relevant Plasmids and Strains

Plasmid Name	Description	Source
pMA1214	*GAL1-CIN8* plasmid	M.A. Hoyt
pMA1186	*cin8Δ* plasmid	M.A. Hoyt
pB1585	3xGFP plasmid	D. Pellman
pRS406	mCherry-*TUB1* plasmid	S. Reed

Strain Name	Description	Source
YEF473A	*MATa trp1-63 leu2-1 ura3-52 his3-200 lys2-801*	J. Pringle
KBY2012	As YEF473A except *cse4::HYG SPC29-CFP-KAN pKK1*	C. Pearson
KBY2270	As YEF473A except *cin8::LEU2 cse4::HYG SPC29-CFP-KAN pKK1*	This Study
KBY2129	As YEF473A except *GFP-TUB1::leu2_1, SPC29RFPKAN*	C. Pearson
KBY2275	As YEF473A except *cin8::LEU2 GFP-TUB1::leu2_1,SPC29RFPKAN*	This study
KBY7001	As YEF473A except *kip1::NAT cse4::HYG SPC29-CFP-KAN pKK1*	This Study
KBY8030A	As YEF473A except *mCherry-TUB1:URA3*	This Study
KBY8023	As YEF473A except *Cin8-GFP:HIS3MX6, NDC80-Cherry:KAN*	This Study
KBY8052	As YEF473A except *CIN8-GFP:HIS3, SPC29RFP:HYG*	This Study
DCB 411.1	As YEF 473A except *CIN8-3GFP-HIS3 mCherry-TUB1-URA3*	This Study
DCB 421.1	As YEF473A except *CIN8-NLSdelta-3GFP-HIS mCherry-TUB1-URA3*	This Study
DCB 430	As YEF473A except *pGAL-CIN8-HIS3 cse4::HYG SPC29-CFP-KAN pKK1*	This Study
KBY8033A	As YEF473A except *pGAL cin8:HIS GFP-TUB1::leu2_1, SPC29RFPKAN*	This Study
DCB 204.1	As YEF473A except *HHT1::TRP1 KAN-GAL1p-HHT2 ura3::NUF2-GFP-URA3 SPC29-RFP HYG*	D. Bouck
DCB 208.1	As YEF473A except *HHT1::TRP1 KAN-GAL1p-HHT2 ura3::NUF2-GFP-URA3 SPC29-CFP-HIS3 cin8::LEU2*	D. Bouck

Supplemental References

Bell, G. I. (1978). Models for the specific adhesion of cells to cells. Science *200*, 618-627.

Bloom, K., Beach, D. L., Maddox, P., Shaw, S. L., Yeh, E., and Salmon, E. D. (1998). Using Green Fluorescent Protein Fusion Proteins to Quantitate Microtubule and Spindle Dynamics in Budding Yeast, In Methods in Cell Biology (San Diego: Academic Press), pp. 369-383.

Bouck, D. C., and Bloom, K. (2007). Pericentric chromatin is an elastic component of the mitotic spindle. Curr Biol *17*, 741-748.

Carminati, J. L., and Stearns, T. (1997). Microtubules orient the mitotic spindle in yeast through dynein-dependent interactions with the cell cortex. J Cell Biol *138*, 629-641.

Evans, E. A., and Calderwood, D. A. (2007). Forces and bond dynamics in cell adhesion. Science *316*, 1148-1153.

Franck, A. D., Powers, A. F., Gestaut, D. R., Gonen, T., Davis, T. N., and Asbury, C. L. (2007). Tension applied through the Dam1 complex promotes microtubule elongation providing a direct mechanism for length control in mitosis. Nat Cell Biol *9*, 832-837.

Gardner, M. K., Haase, J., Mythreye, K., Molk, J. N., Anderson, M., Joglekar, A. P., O'Toole, E. T., Winey, M., Salmon, E. D., Odde, D. J., and Bloom, K. (2008). The microtubule-based motor Kar3 and plus end-binding protein Bim1 provide structural support for the anaphase spindle. J Cell Biol *180*, 91-100.

Gardner, M. K., Pearson, C. G., Sprague, B. L., Zarzar, T. R., Bloom, K., Salmon, E. D., and Odde, D. J. (2005). Tension-dependent Regulation of Microtubule Dynamics at Kinetochores Can Explain Metaphase Congression in Yeast. Mol Biol Cell *16*, 3764-3775.

Gheber, L., Kuo, S. C., and Hoyt, M. A. (1999). Motile properties of the kinesin-related Cin8p spindle motor extracted from Saccharomyces cerevisiae cells. J Biol Chem *274*, 9564-9572.

Gordon, D. M., and Roof, D. M. (1999). The kinesin-related protein Kip1p of Saccharomyces cerevisiae is bipolar. J Biol Chem *274*, 28779-28786.

Goshima, G., and Yanagida, M. (2000). Establishing Biorientation Occurs with Precocious Separation of the Sister Kinetochores, but Not the Arms, in the Early Spindle of Budding Yeast. Cell *100*, 619-633.

Goshima, G., and Yanagida, M. (2001). Time course analysis of precocious separation of sister centromeres in budding yeast: continuously separated or frequently reassociated? Genes Cells *6*, 765-773.

Gupta, M. L., Jr., Bode, C. J., Thrower, D. A., Pearson, C. G., Suprenant, K. A., Bloom, K. S., and Himes, R. H. (2002). beta-Tubulin C354 mutations that severely decrease microtubule dynamics do not prevent nuclear migration in yeast. Mol Biol Cell *13*, 2919-2932.

Gupta, M. L., Jr., Carvalho, P., Roof, D. M., and Pellman, D. (2006). Plus end-specific depolymerase activity of Kip3, a kinesin-8 protein, explains its role in positioning the yeast mitotic spindle. Nat Cell Biol *8*, 913-923.

Hancock, W. O., and Howard, J. (1998). Processivity of the motor protein kinesin requires two heads. J Cell Biol *140*, 1395-1405.

He, X., Asthana, S., and Sorger, P. K. (2000). Transient Sister Chromatid Separation and Elastic Deformation of Chromosomes during Mitosis in Budding Yeast. Cell *101*, 763-775.

Hildebrandt, E. R., and Hoyt, M. A. (2000). Mitotic motors in Saccharomyces cerevisiae. Biochim Biophys Acta *1496*, 99-116.

Hildebrandt, E. R., and Hoyt, M. A. (2001). Cell cycle-dependent degradation of the Saccharomyces cerevisiae spindle motor Cin8p requires APC(Cdh1) and a bipartite destruction sequence. Mol Biol Cell *12*, 3402-3416.

Hunt, A. J., and Howard, J. (1993). Kinesin swivels to permit microtubule movement in any direction. Proc Natl Acad Sci U S A *90*, 11653-11657.

Joglekar, A. P., Bouck, D. C., Molk, J. N., Bloom, K. S., and Salmon, E. D. (2006). Molecular architecture of a kinetochore-microtubule attachment site. Nat Cell Biol *8*, 581-585.

Kapitein, L. C., Peterman, E. J., Kwok, B. H., Kim, J. H., Kapoor, T. M., and Schmidt, C. F. (2005). The bipolar mitotic kinesin Eg5 moves on both microtubules that it crosslinks. Nature *435*, 114-118.

Kashina, A. S., Baskin, R. J., Cole, D. G., Wedaman, K. P., Saxton, W. M., and Scholey, J. M. (1996). A bipolar kinesin. Nature *379*, 270-272.

Kawaguchi, K., and Ishiwata, S. (2001). Nucleotide-dependent single- to double-headed binding of kinesin. Science *291*, 667-669.

King, J. M., and Nicklas, R. B. (2000). Tension on chromosomes increases the number of kinetochore microtubules but only within limits. J Cell Sci *113 Pt 21*, 3815-3823.

Korneev, M. J., Lakamper, S., and Schmidt, C. F. (2007). Load-dependent release limits the processive stepping of the tetrameric Eg5 motor. Eur Biophys J *36*, 675-681.

Kuo, S. C., Gelles, J., Steuer, E., and Sheetz, M. P. (1991). A model for kinesin movement from nanometer-level movements of kinesin and cytoplasmic dynein and force measurements. Journal of Cell Science - Supplement *14*, 135-138.

Lee, G., Abdi, K., Jiang, Y., Michaely, P., Bennett, V., and Marszalek, P. E. (2006). Nanospring behaviour of ankyrin repeats. Nature *440*, 246-249.

Maddox, P., Bloom, K., and Salmon, E. D. (2000). Polarity and Dynamics of Microtubule Assembly in the Budding Yeast *Saccharomyces cerevisiae*. Nature Cell Biology *2*, 36-41.

Northrup, S. H., and Erickson, H. P. (1992). Kinetics of protein-protein association explained by Brownian dynamics computer simulation. Proc Natl Acad Sci U S A *89*, 3338-3342.

O'Toole, E. T., Winey, M., and McIntosh, J. R. (1999). High-voltage electron tomography of spindle pole bodies and early mitotic spindles in the yeast Saccharomyces cerevisiae. Molecular Biology of the Cell *10*, 2017-2031.

Odde, D. J., and Hawkins, S. S. (1997). Computer-Assisted Motion Analysis of Fluorescent Tubulin Dynamics in the Nerve Growth Cone. Journal of Computer-Assisted Microscopy *9*, 143-151.

Pearson, C. G., Gardner, M. K., Paliulis, L. V., Salmon, E. D., Odde, D. J., and Bloom, K. (2006). Measuring Nanometer Scale Gradients in Spindle Microtubule Dynamics Using Model Convolution Microscopy. Mol Biol Cell *17*, 4069-4079.

Pearson, C. G., Maddox, P. S., Salmon, E. D., and Bloom, K. (2001). Budding Yeast Chromosome Structure and Dynamics during Mitosis. J Cell Biol *152*, 1255-1266.

Pearson, C. G., Maddox, P. S., Zarzar, T. R., Salmon, E. D., and Bloom, K. (2003). Yeast kinetochores do not stabilize Stu2p-dependent spindle microtubule dynamics. Mol Biol Cell *14*, 4181-4195.

Pearson, C. G., Yeh, E., Gardner, M., Odde, D., Salmon, E. D., and Bloom, K. (2004). Stable kinetochore-microtubule attachment constrains centromere positioning in metaphase. Curr Biol *14*, 1962-1967.

Roof, D. M., Meluh, P. B., and Rose, M. D. (1992). Kinesin-related proteins required for assembly of the mitotic spindle. Journal of Cell Biology *118*, 95-108.

Saunders, W., Lengyel, V., and Hoyt, M. A. (1997). Mitotic Spindle Function in Saccharomyces cerevisiae Requires a Balance between Different Types of Kinesin-related Motors. Molecular biology of the cell *8*, 1025-1033.

Shimogawa, M. M., Graczyk, B., Gardner, M. K., Francis, S. E., White, E. A., Ess, M., Molk, J. N., Ruse, C., Niessen, S., Yates, J. R., 3rd*, et al.* (2006). Mps1 phosphorylation

of dam1 couples kinetochores to microtubule plus ends at metaphase. Curr Biol *16*, 1489-1501.

Sprague, B. L., Pearson, C. G., Maddox, P. S., Bloom, K. S., Salmon, E. D., and Odde, D. J. (2003). Mechanisms of Microtubule-Based Kinetochore Positioning in the Yeast Metaphase Spindle. Biophys J *84*, 1-18.

Tanaka, K., Mukae, N., Dewar, H., van Breugel, M., James, E. K., Prescott, A. R., Antony, C., and Tanaka, T. U. (2005). Molecular mechanisms of kinetochore capture by spindle microtubules. Nature *434*, 987-994.

Tao, L., Mogilner, A., Civelekoglu-Scholey, G., Wollman, R., Evans, J., Stahlberg, H., and Scholey, J. M. (2006). A homotetrameric kinesin-5, KLP61F, bundles microtubules and antagonizes Ncd in motility assays. Curr Biol *16*, 2293-2302.

Tytell, J. D., and Sorger, P. K. (2006). Analysis of kinesin motor function at budding yeast kinetochores. J Cell Biol *172*, 861-874.

Valentine, M. T., Fordyce, P. M., Krzysiak, T. C., Gilbert, S. P., and Block, S. M. (2006). Individual dimers of the mitotic kinesin motor Eg5 step processively and support substantial loads in vitro. Nat Cell Biol *8*, 470-476.

Winey, M., Mamay, C. L., O'Toole, E. T., Mastronarde, D. N., Giddings, T. H., Jr., McDonald, K. L., and McIntosh, J. R. (1995). Three-dimensional ultrastructural analysis of the Saccharomyces cerevisiae mitotic spindle. Journal of Cell Biology *129*, 1601-1615.